

Aerosol assisted chemical vapour deposition of MoO₃ and MoO₂ thin films on glass from molybdenum polyoxometallate precursors; thermophoresis and gas phase nanoparticle formation

Sobia Ashraf, Christopher S. Blackman, Geoffrey Hyett and Ivan P. Parkin*

Received 24th May 2006, Accepted 24th July 2006

First published as an Advance Article on the web 8th August 2006

DOI: 10.1039/b607335b

Aerosol assisted chemical vapour deposition (AACVD) of molybdenum polyoxometallates dissolved in acetonitrile or water yielded adhesive thin films of molybdenum oxides on glass. At substrate temperatures of 300–350 °C single phase MoO₃ was obtained, from 350–500 °C mixed phases of MoO₃–MoO₂ were formed and at 500–550 °C single phase MoO₂ was observed. The morphology of the as-deposited molybdenum oxide films was found to be dependent upon a number of factors including the nature of the precursor used, the deposition temperature and position of the film within the reactor. Needles, spheres, agglomerates and platelets formed depending on the conditions. The films with a needle-like microstructure displayed enhanced hydrophobicity to water droplets (125° contact angle). X-Ray diffraction showed that the MoO₃ films had typical cell constants of $a = 3.96$, $b = 13.85$, $c = 3.69$ Å and the MoO₂ films had typical cell constants of $a = 5.62$, $b = 4.84$, $c = 5.56$ Å, $\beta = 119.32^\circ$. The MoO₂ films were readily converted to MoO₃ by annealing in air for 30 minutes at 600 °C. The MoO₃ films functioned as gas sensors showing a linear change in electrical resistance upon exposure to trace amounts of ethanol vapour in air.

Introduction

Molybdenum oxide thin films have applications in a diverse range of fields including electrochromic devices, catalysis and as gas sensor components.^{1–5} The gas sensing properties arise due to changes in electrical conductivity upon adsorption of trace gases onto the semiconductor surface.¹ Molybdenum oxide thin films have been deposited from a variety of techniques including sol–gel,² spin-coating,³ electrochemical deposition,⁴ spray pyrolysis,⁵ flash and thermal evaporation,⁶ physical vapour deposition (PVD),⁷ combustion CVD (CCVD)¹ and hot filament metal oxide deposition (HFMOD).⁸ All of these methods involved the use of small molecular precursors typically containing a single molybdenum atom. Molybdenum oxide thin films have been deposited from dual-source CVD reactions of molybdenum hexacarbonyl and oxygen and from single source precursors such as molybdenum pentacarbonyl 1-methylbutylisonitrile.⁹ The structure, phase and properties of the resulting films are strongly dependent upon the deposition technique employed.

Aerosol assisted chemical vapour deposition (AACVD) is a variant of the CVD process involving the use of liquid–gas aerosols to transport soluble precursors to a heated substrate. The method has traditionally been used when a conventional atmospheric pressure CVD precursor proves involatile or thermally unstable. However, by designing precursors specifically for AACVD, the restrictions of volatility and thermal stability are eliminated, and new precursors and films can be investigated. Ionic precursors such as sodium fluoride have

been used in aerosol-assisted depositions of thin films.^{10,11} In this paper we present the deposition, analysis and functional properties of molybdenum oxide films from AACVD using polyoxometallates, large charged clusters formed by the early transition metals in high oxidation states. Polyoxometallates are the antithesis of conventional CVD precursors, which tend to be molecular, volatile non-ionic complexes. The main advantage of polyoxometallates as CVD precursors is their relatively low temperatures required for clean decomposition to the corresponding metal oxide (300–500 °C). Furthermore molybdenum polyoxometallates containing hetero-atoms, such as phosphorus, vanadium, niobium and tungsten, are easy to prepare, and provide a convenient route to incorporating a secondary element into the molybdenum oxide films.^{12,13} We have shown previously in a communication that polytungstates can be used as AACVD precursors for the deposition of tungsten oxide films.¹¹ Here we show that the approach can be extended to include polyoxomolybdates and hence demonstrate the versatility of polyoxometallates as AACVD precursors.

Experimental

The polyoxomolybdates [¹⁸Bu₄N]₄[Mo₈O₂₆], [¹⁸Bu₄N]₂[Mo₂O₇], [¹⁸Bu₄N]₄[Mo₈O₂₆] and [¹⁸Bu₄N]₃[PMo₁₂O₄₀] were synthesised according to the literature procedure¹² and [NH₄]₆[Mo₇O₂₄] was purchased from Aldrich and used without further refinement. Nitrogen (99.99%) was obtained from BOC and used as supplied. Coatings were deposited on 150 mm × 45 mm × 4 mm sheets of SiO₂ coated float-glass (the SiO₂ acts a blocking layer preventing diffusion of ions from within the glass into the deposited film), which was supplied by

Department of Chemistry, University College London, 20 Gordon Street, London, UK WC1H 0AJ

Pilkington Glass Plc. The glass was cleaned prior to use by washing with acetone and propan-2-ol and then dried in air. The glass substrate was heated on a graphite block containing a Whatman cartridge heater in a horizontal-bed cold-wall AACVD reactor. The temperature of the graphite block was monitored by Pt–Rh thermocouples. Measurements indicated that temperature gradients of less than 25 °C at 500 °C were noted across the glass substrates. All gas-handling lines were made of stainless steel and were of 1/4 in internal diameter, except for the inlet to the mixing chamber and the exhaust line from the apparatus, which were 1/2 in i.d.

General synthesis procedure

The polyoxometallate precursors (0.25 g) were dissolved in 50 ml of acetonitrile (except $[\text{NH}_4]_6[\text{Mo}_7\text{O}_{24}]$ which was used in water) and an aerosol was generated at room temperature using a PIFCO ultrasonic humidifier. Nitrogen was passed through the aerosol mist, forcing the aerosol droplets laden with precursor into the reactor chamber (Table 1). The exhaust from the reactor was vented directly into the extraction system of a fume cupboard. Deposition experiments were conducted by heating the horizontal bed reactor to the required temperatures before diverting the nitrogen line through the aerosol into the reactor. The gas flow was continued until all the precursor mix had passed through the reactor, typically 30–60 minutes. Films were cooled to room temperature *in situ* under a flow of nitrogen and after cooling were stored and handled in air.

Film analysis

X-Ray diffraction (XRD) patterns were recorded using a Bruker D8 discover reflection diffractometer, with Cu-K_α radiation ($\lambda = 1.5406 \text{ \AA}$) in reflection mode with a glancing

angle incidence beam (5°). Scanning electron microscopy (SEM) was carried out on a field emission JEOL 6301F instrument. Wavelength dispersive X-ray analysis (WDX) was carried out on a Philips ESEM with an Oxford INCA system. Samples were coated with gold to improve conductivity and images were recorded digitally. X-Ray photoelectron spectroscopy (XPS) measurements were carried out on a VG ESALAB 220i XL instrument using focussed (300 μm spot) monochromatic Al-K_α X-ray radiation at a pass energy of 20 eV. Scans were acquired with steps of 50 meV. A flood gun was used to control charging and the binding energies were referenced to surface elemental carbon at 284.6 eV. Raman spectra were acquired on a Renishaw Raman System 1000 using a helium–neon laser of wavelength 632.8 nm. The Raman system was calibrated against the emission lines of neon. Differential scanning calorimetry (DSC)/thermal gravimetric analysis (TGA) was performed using a NETZSCH STA 449 instrument from 20 °C to 550 °C at a heating rate of 10 K min^{-1} , with the samples stored under nitrogen in aluminium crucibles. Hardness scratch tests were conducted with a stainless steel scalpel. Contact angle measurements for water droplets were determined by measuring the spread of a known volume of water on the surface.

Gas sensor measurements

The sensor substrates were made of alumina tiles with interdigitated gold electrodes on the top and a platinum strip on the back, which serves as a microheater. The platinum heater track of each sensor also formed one arm of a Wheatstone bridge, which allowed the resistance, and hence the heater temperature, to be both regulated and programmed.

The gas sensing setup comprised a stainless steel test chamber to which gases (BOC special gases) were streamed

Table 1 Deposition temperatures, gas flow rates and phases seen by XRD and Raman for the AACVD of molybdenum polyoxometallate precursors on glass. Phases separated by commas indicate that sections of the substrate contained separate phases, entries such as $\text{MoO}_2/\text{MoO}_3$ indicate that both phases coexisted in the same region of the substrate

Precursor	Substrate temp./°C	N_2 Flow rate/ l min^{-1}	XRD	Raman
$[\text{Bu}_4\text{N}]_4[\text{Mo}_8\text{O}_{26}]$	550	1	MoO_2	MoO_2
$[\text{Bu}_4\text{N}]_4[\text{Mo}_8\text{O}_{26}]$	500	0.5	MoO_2	MoO_2
$[\text{Bu}_4\text{N}]_4[\text{Mo}_8\text{O}_{26}]$	450	0.5	MoO_3 , MoO_2 , $\text{MoO}_2/\text{MoO}_3$	MoO_3 , MoO_2 , $\text{MoO}_2/\text{MoO}_3$
$[\text{Bu}_4\text{N}]_4[\text{Mo}_8\text{O}_{26}]$	400	0.5	MoO_3 , $\text{MoO}_2/\text{MoO}_3$	MoO_3
$[\text{Bu}_4\text{N}]_4[\text{Mo}_8\text{O}_{26}]$	350	0.5	MoO_3 , $\text{MoO}_2/\text{MoO}_3$	MoO_3 , $\text{MoO}_2/\text{MoO}_3$
$[\text{Bu}_4\text{N}]_4[\text{Mo}_8\text{O}_{26}]$	300	0.5	MoO_3	MoO_3
$[\text{Bu}_4\text{N}]_2[\text{Mo}_2\text{O}_7]$	500	0.5	$\text{MoO}_2/\text{MoO}_3$	$\text{MoO}_2/\text{MoO}_3$
$[\text{Bu}_4\text{N}]_2[\text{Mo}_2\text{O}_7]$	450	0.5	$\text{MoO}_2/\text{MoO}_3$	$\text{MoO}_2/\text{MoO}_3$
$[\text{Bu}_4\text{N}]_2[\text{Mo}_2\text{O}_7]$	400	0.5	$\text{MoO}_2/\text{MoO}_3$	$\text{MoO}_2/\text{MoO}_3$
$[\text{Bu}_4\text{N}]_2[\text{Mo}_2\text{O}_7]$	350	0.5	$\text{MoO}_2/\text{MoO}_3$	$\text{MoO}_2/\text{MoO}_3$
$[\text{Bu}_4\text{N}]_4[\text{Mo}_6\text{O}_{19}]$	550	0.5	MoO_2	MoO_2
$[\text{Bu}_4\text{N}]_4[\text{Mo}_6\text{O}_{19}]$	500	0.5	$\text{MoO}_2/\text{MoO}_3$	$\text{MoO}_2/\text{MoO}_3$
$[\text{Bu}_4\text{N}]_4[\text{Mo}_6\text{O}_{19}]$	450	0.5	$\text{MoO}_2/\text{MoO}_3$	$\text{MoO}_2/\text{MoO}_3$
$[\text{Bu}_4\text{N}]_4[\text{Mo}_6\text{O}_{19}]$	400	0.5	$\text{MoO}_2/\text{MoO}_3$	$\text{MoO}_2/\text{MoO}_3$
$[\text{Bu}_4\text{N}]_4[\text{Mo}_6\text{O}_{19}]$	350	0.5	$\text{MoO}_2/\text{MoO}_3$	$\text{MoO}_2/\text{MoO}_3$
$[\text{Bu}_4\text{N}]_4[\text{Mo}_6\text{O}_{19}]$	300	0.5	MoO_3	MoO_3
$[\text{NH}_4]_6[\text{Mo}_7\text{O}_{24}]$	450	2	$\text{MoO}_2/\text{MoO}_3$	$\text{MoO}_2/\text{MoO}_3$
$[\text{NH}_4]_6[\text{Mo}_7\text{O}_{24}]$	400	2	$\text{MoO}_2/\text{MoO}_3$	$\text{MoO}_2/\text{MoO}_3$
$[\text{Bu}_4\text{N}]_3[\text{PMo}_{12}\text{O}_{40}]$	550	1	MoO_2	MoO_3
$[\text{Bu}_4\text{N}]_3[\text{PMo}_{12}\text{O}_{40}]$	500	1	$\text{MoO}_3/\text{MoP}_2\text{O}_7$	MoO_2
$[\text{Bu}_4\text{N}]_3[\text{PMo}_{12}\text{O}_{40}]$	450	2	$\text{MoO}_3/\text{MoO}_2/\text{MoP}_2\text{O}_7$	$\text{MoO}_2/\text{MoO}_3$
$[\text{Bu}_4\text{N}]_3[\text{PMo}_{12}\text{O}_{40}]$	450	1	$\text{MoO}_3/\text{MoP}_2\text{O}_7$	$\text{MoO}_2/\text{MoO}_3$
$[\text{Bu}_4\text{N}]_3[\text{PMo}_{12}\text{O}_{40}]$	400	1	$\text{MoO}_3/\text{MoP}_2\text{O}_7$	MoO_3
$[\text{Bu}_4\text{N}]_3[\text{PMo}_{12}\text{O}_{40}]$	350	1	amorphous	MoO_3

through PC controlled mass flow controllers (Tylan General). Two terminal resistance measurements in varying gas atmospheres were performed using an in-house constructed test-rig that has been described previously.¹³ The devices were initially allowed to stabilize for 24 hours at their operating temperatures before any measurements were taken. Automated resistance readings were made every 60 s with a multiplexed Keithley Digital Multimeter.

Results and discussion

Aerosol assisted chemical vapour deposition of five polyoxometallate precursors: $[(n-C_4H_9)_4N]_4[Mo_8O_{26}]$; $[(n-C_4H_9)_4N]_4[Mo_2O_7]$; $[(n-C_4H_9)_4N]_4[Mo_6O_{19}]$; $[NH_4]_6[Mo_7O_{24}]$ and $[(n-C_4H_9)_4N]_3[PMo_{12}O_{40}]$, using acetonitrile or water as a solvent and transport medium were studied at substrate deposition temperatures of 300–550 °C. The coatings were deposited exclusively on the upper substrate of a cold wall CVD reactor.¹¹ The upper substrate (not directly heated) was placed 4 mm above and was measured to be 50–75 °C colder than the bottom plate. The temperature measurements given in this work, Table 1 and the text of this paper, relate to the upper substrate temperature. This somewhat unusual deposition site arises from the relatively large size of the polyoxometallate clusters coupled with gas phase nucleation effects. Gas phase particles are subject to a thermophoretic force when exposed to a temperature gradient.¹⁴ This force is directed away from the hot surface, so larger particles act as if repelled from a hot surface and attracted towards a colder one. In effect the larger particles cannot diffuse through the thermal boundary layer at the surface of the hotter substrate. Since the flow of gas in the reactor is laminar rather than turbulent, thermophoresis is usually the dominant force in determining the deposition location of particles; hence coatings were obtained exclusively on the top plate. Similar effects have been observed in AACVD using nanoparticles.¹⁵ At deposition temperatures in excess of 500 °C deep blue films were formed whereas lower reaction temperatures resulted in the deposition of white coatings. The films were adherent passing the Scotch tape test. At 350–500 °C and irrespective of the polyoxometallate used the films were comprised of multiple regions, a well adhered deep-blue film, an adherent white coating and a powdery black/blue surface deposit.

Complete coverage of the substrate was obtained at deposition temperatures below 400 °C with less coverage observed at higher temperatures, the films having full-width coverage but being localised to the central third of the substrate. This form of deposition often relates to depletion of the precursor in the carrier gas stream due to faster reaction rates at higher temperature, in effect a mass transport limited deposition.

Film characterisation

Raman analysis. The Raman spectra recorded for the molybdenum polyoxometallate precursors showed similar variations in phase with increasing substrate temperature. At 300 °C films were comprised solely of the MoO_3 phase whereas at the highest deposition temperatures of 500–550 °C single phase MoO_2 was observed. At intermediate substrate

temperatures of 350–500 °C mixed phase MoO_2/MoO_3 films were obtained. These mixed phase films showed good coverage of the substrate, however for some depositions, in particular those using $[{}^nBu_4N]_4[Mo_8O_{26}]$, the substrate was comprised of at least two distinct regions: an adherent white portion closest to the precursor inlet which had a Raman spectrum characteristic of only MoO_3 and a dark blue region further away from the precursor inlet which displayed additional bands due to MoO_2 . This variation in the ratio of MoO_2 to MoO_3 was also observed for the entirely mixed phase films listed as MoO_3/MoO_2 in Table 1, with the MoO_2 phase predominating with increasing distance from the precursor inlet. The Raman spectra for the films deposited at 400 °C from the AACVD reactions of $[{}^nBu_4N]_4[Mo_8O_{26}]$ and $[{}^nBu_4N]_4[Mo_6O_{19}]$ are shown in Fig. 1. The film deposited from $[{}^nBu_4N]_4[Mo_8O_{26}]$ has a Raman pattern characteristic of orthorhombic MoO_3 with bands at 282, 337, 665, 822 and 996 cm^{-1} . The Raman spectrum for the film obtained from $[{}^nBu_4N]_4[Mo_6O_{19}]$ displayed additional bands due to the monoclinic MoO_2 phase at 474, 562 and 681 cm^{-1} .¹⁶

X-Ray diffraction. Glancing angle X-ray diffraction (XRD) was used to analyse the films. By using a small focused X-ray spot (1–2 mm^2) at low incident angle it was possible to analyse separate regions of the films and obtain X-ray profiles of the substrate at different points along its length. This variation in the oxide phase deposited along the length of the substrate is illustrated well by the film deposited from $[{}^nBu_4N]_4[Mo_8O_{26}]$ at 450 °C and 0.5 $l\ min^{-1}$. The film is comprised of approximately six regions varying in colour. The XRD patterns of the different regions are shown in Fig. 2. The region closest to the precursor inlet is comprised solely of MoO_3 and that furthest away of MoO_2 . The intermediate regions consist of a mixture of these two phases representing a transition from the trioxide to the dioxide. Films deposited from $[{}^nBu_4N]_4[Mo_8O_{26}]$ at

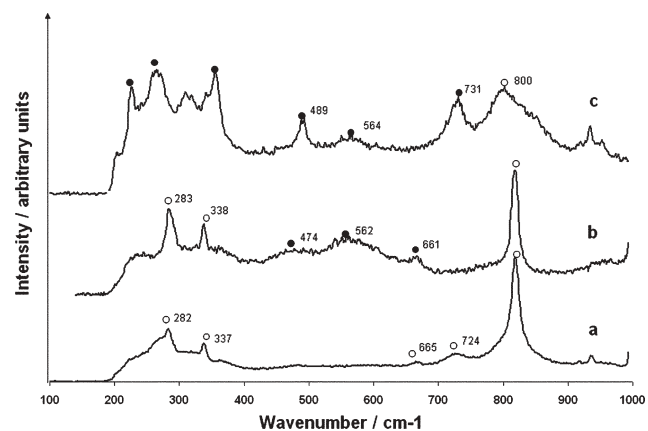


Fig. 1 Raman spectra for films deposited from $[{}^nBu_4N]_4[Mo_8O_{26}]$, a, and $[{}^nBu_4N]_4[Mo_6O_{19}]$, b, in acetonitrile at 450 °C and 0.5 $l\ min^{-1}$. The spectrum of a is characteristic of molybdenum trioxide (hollow circles) whereas that of b contains additional peaks due to the dioxide phase (filled circles). Spectrum c shows the Raman pattern of the film deposited from $[{}^nBu_4N]_4[Mo_8O_{26}]$ at 550 °C which is characteristic of molybdenum dioxide, with the exception of the broad peak in the region 800 cm^{-1} , which may be a consequence of the high laser power or due to a more oxidised surface compared with the bulk of the film.

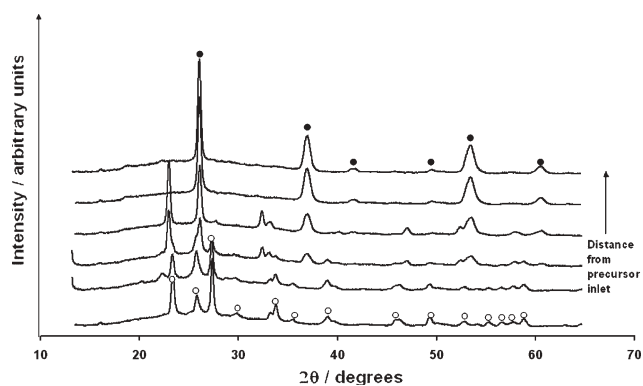


Fig. 2 Powder XRD patterns for the film deposited by the AACVD reaction of $[\text{tBu}_4\text{N}]_4[\text{Mo}_8\text{O}_{26}]$ in acetonitrile at $450\text{ }^\circ\text{C}$ and 0.5 l min^{-1} as a function of distance from the precursor inlet. The stack plot illustrates the predominance of the molybdenum dioxide phase (filled circles) over the molybdenum trioxide phase (hollow circles) with increasing temperature.

$400\text{ }^\circ\text{C}$ also have variable composition (Table 1). In contrast the films obtained at $500\text{ }^\circ\text{C}$ and $550\text{ }^\circ\text{C}$ consisted solely of the MoO_2 phase. The single phase MoO_3 and MoO_2 films showed no preferential orientation, whereas the MoO_3 components of the mixed phase films did show some degree of preferred orientation. However due to the overlap of peaks it was not possible to determine the plane of orientation. Preferred orientation arises when the constraints of a thin film are imposed upon a material, and is a feature commonly associated with CVD films.

The X-ray diffraction data is consistent with the Raman study; at substrate temperatures of $550\text{ }^\circ\text{C}$ and $500\text{ }^\circ\text{C}$ the diffraction patterns are characteristic of monoclinic MoO_2 , at $300\text{ }^\circ\text{C}$ and $350\text{ }^\circ\text{C}$ of orthorhombic MoO_3 whereas those obtained at intermediate temperatures relate to a mixture of the two oxide phases. However the observation of a predominantly MoO_2 phase for the films deposited at $450\text{ }^\circ\text{C}$ from $[\text{tBu}_4\text{N}]_4[\text{Mo}_8\text{O}_{26}]$ contradicts with the Raman data, in which MoO_3 was also observed. This difference may be due to oxidation of the films at high laser powers or a consequence of the surface sensitivity of the technique compared with XRD. The diffraction patterns for MoO_3 indexed in the $Pbmm$ space group with typical cell parameters of $a = 3.96$, $b = 13.85$, $c = 3.69\text{ \AA}$; this compares with literature values of $a = 3.92$, $b = 13.94$, $c = 3.66\text{ \AA}$,¹⁷ whereas the MoO_2 diffraction pattern indexed in the $P12_11$ space group with typical cell parameters of $a = 5.62$, $b = 4.84$, $c = 5.56\text{ \AA}$, $\beta = 119.32^\circ$ which again compares very well with typical literature values of $a = 5.61$, $b = 4.84$, $c = 5.53\text{ \AA}$, $\beta = 119.62^\circ$.¹⁸ The coatings obtained from $[\text{tBu}_4\text{N}]_4[\text{Mo}_8\text{O}_{26}]$ at a given deposition temperature were the most crystalline in nature (as calculated from XRD line broadening studies) followed by those deposited from $[\text{tBu}_4\text{N}]_3[\text{PMO}_{12}\text{O}_{40}]$ and those from $[\text{tBu}_4\text{N}]_2[\text{Mo}_2\text{O}_7]$ and $[\text{tBu}_4\text{N}]_4[\text{Mo}_6\text{O}_{19}]$ were the least. For example the coatings deposited from $[\text{tBu}_4\text{N}]_4[\text{Mo}_8\text{O}_{26}]$ and $[\text{tBu}_4\text{N}]_3[\text{PMO}_{12}\text{O}_{40}]$ at $400\text{ }^\circ\text{C}$ yielded an MoO_3 phase with crystallite sizes of 310 \AA and 200 \AA respectively (determined using the Scherrer equation). This difference in crystallinity to a certain extent correlates with the temperature changes associated with

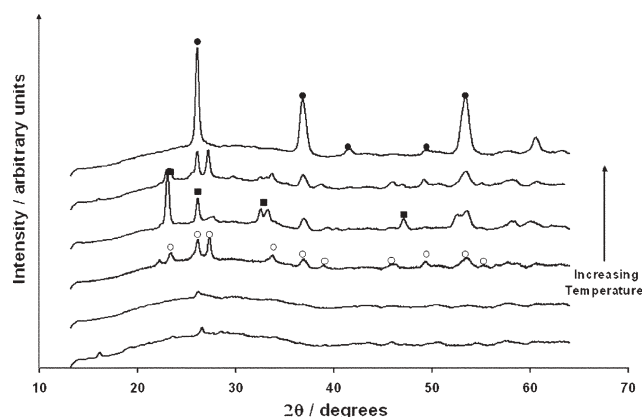


Fig. 3 Powder XRD patterns for the films obtained from the AACVD reactions of $[\text{tBu}_4\text{N}]_3[\text{PMO}_{12}\text{O}_{40}]$ in acetonitrile at varying substrate temperatures. The stack plot illustrates the predominance of the molybdenum dioxide phase (filled circles) over the molybdenum trioxide phase (hollow circles) with increasing deposition temperature. The filled squares represent the peaks arising due to the MoP_2O_7 phase.

molybdenum oxide formation and the crystallisation isotherms as assessed from the TGA/DSC data (see below). Films deposited from $[\text{tBu}_4\text{N}]_3[\text{PMO}_{12}\text{O}_{40}]$ at 400 and $450\text{ }^\circ\text{C}$ contained additional peaks in their XRD spectra which could be assigned to cubic MoP_2O_7 . A stack plot showing the variation in phase as a function of deposition temperature is shown in Fig. 3 for films deposited using $[\text{tBu}_4\text{N}]_3[\text{PMO}_{12}\text{O}_{40}]$.

Thermal gravimetric analysis, differential scanning calorimetry. The TGA/DSC data shows that the polyoxometallates all follow the same general decomposition pattern, Fig. 4, 5. The initial step involves loss of the tetrabutylammonium attendant counter ion to yield the core cluster that upon further heating decomposes to MoO_3 . The final step involves the decomposition of MoO_3 to MoO_2 . This is illustrated for $[\text{tBu}_4\text{N}]_3[\text{PMO}_{12}\text{O}_{40}]$ (Fig. 4) which showed a total mass loss at $500\text{ }^\circ\text{C}$ of 46% that corresponds to decomposition to MoO_2 (theoretically a 45% mass loss). Four distinct decomposition steps are present, and these are interpreted as follows. The first mass loss at $20\text{--}100\text{ }^\circ\text{C}$ corresponds to removal of solvent from the polyoxometallate cluster. From $240\text{--}355\text{ }^\circ\text{C}$ a 28% mass

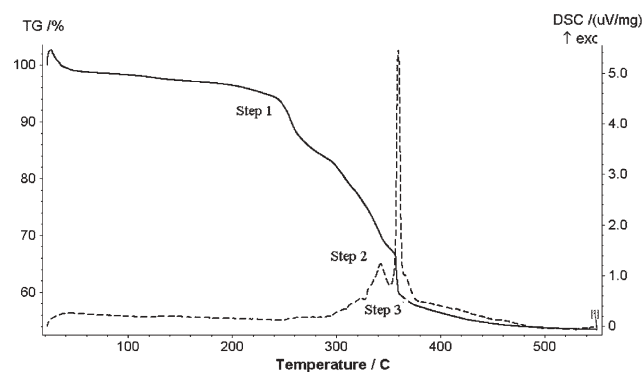


Fig. 4 TGA/DSC data for $[\text{tBu}_4\text{N}]_3[\text{PMO}_{12}\text{O}_{40}]$. Step 1 represents loss of $[\text{tBu}_4\text{N}]_4$ to yield $\text{PMO}_{12}\text{O}_{40}$, step 2 decomposition to MoO_3 and step 3 the conversion to MoO_2 .

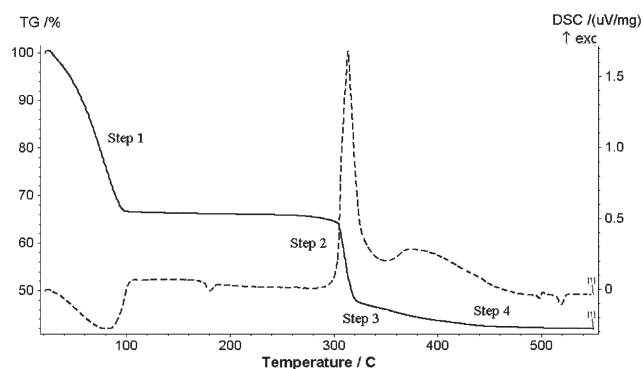


Fig. 5 TGA/DSC data for $[\text{Bu}_4\text{N}]_4[\text{Mo}_8\text{O}_{26}]$. Step 1 represents removal of solvent from the complex, Step 2 represents loss of $[\text{Bu}_4\text{N}]_4$ to yield Mo_8O_{26} , step 3 decomposition to MoO_3 and step 4 the conversion of MoO_3 to MoO_2 .

loss occurs, corresponding to the loss of the three tetrabutylammonium ions (theoretically 28%). From 355–360 °C, a 5% mass loss occurs, corresponding to the decomposition of the $[\text{PMo}_{12}\text{O}_{40}]^{3-}$ core to 12MoO_3 (theoretically 5%). This is associated with a sharp exotherm at 360 °C, indicating the formation of MoO_3 . From 360–500 °C, a 6% mass loss occurs, corresponding to the decomposition of MoO_3 to MoO_2 (theoretically 7%). This final change is accompanied by a broad exotherm.

Scanning electron microscopy and wavelength dispersive analysis by X-rays. Scanning electron microscopy (SEM) was used to examine the surface morphology of the films and measure the film thickness. The microstructure of the deposited films varied greatly as a function of the precursor, the deposition temperature and position of the film on the substrate. Deposition from $[\text{Bu}_4\text{N}]_4[\text{Mo}_8\text{O}_{26}]$ at 400 °C afforded a material that is comprised of spherical agglomerates of crystallites up to 1 μm in diameter, intertwined with needle agglomerates, Fig. 6, images 1 and 2. The film deposited from the same precursor at 500 °C yielded a coating with a similar microstructure; however there appears to be a greater concentration of needle agglomerates (images 3 and 4). These morphologies are consistent with the formation of multi-phase films, with the spherical agglomerates representing the trioxide phase, whereas the needle agglomerates correlate to MoO_2 . This trend was observed for many of the coatings deposited from $[\text{Bu}_4\text{N}]_4[\text{Mo}_8\text{O}_{26}]$; regions of the films in which the dioxide phase predominated contained a higher concentration of the needle agglomerates. Annealing the films in air at 550 or 600 °C resulted in a film microstructure composed entirely of spherical agglomerates or of a condensed continuous film. Deposition from $[\text{Bu}_4\text{N}]_2[\text{Mo}_2\text{O}_7]$, $[\text{Bu}_4\text{N}]_4[\text{Mo}_6\text{O}_{19}]$ and $(\text{NH}_4)_6[\text{Mo}_7\text{O}_{24}]$ at 500 °C (images 6, 7 and 8 respectively) afforded a material comprised of agglomerates of crystallites up to 1 μm in diameter, with a greater degree of agglomeration observed for the films deposited from $[\text{Bu}_4\text{N}]_2[\text{Mo}_2\text{O}_7]$ and $[\text{Bu}_4\text{N}]_4[\text{Mo}_6\text{O}_{19}]$, whereas the coating obtained from $[\text{Bu}_4\text{N}]_3[\text{PMo}_{12}\text{O}_{40}]$ at the same temperature was composed of needles and platelets up to 1 μm in length fused together (image 9). These morphologies obtained in this study are

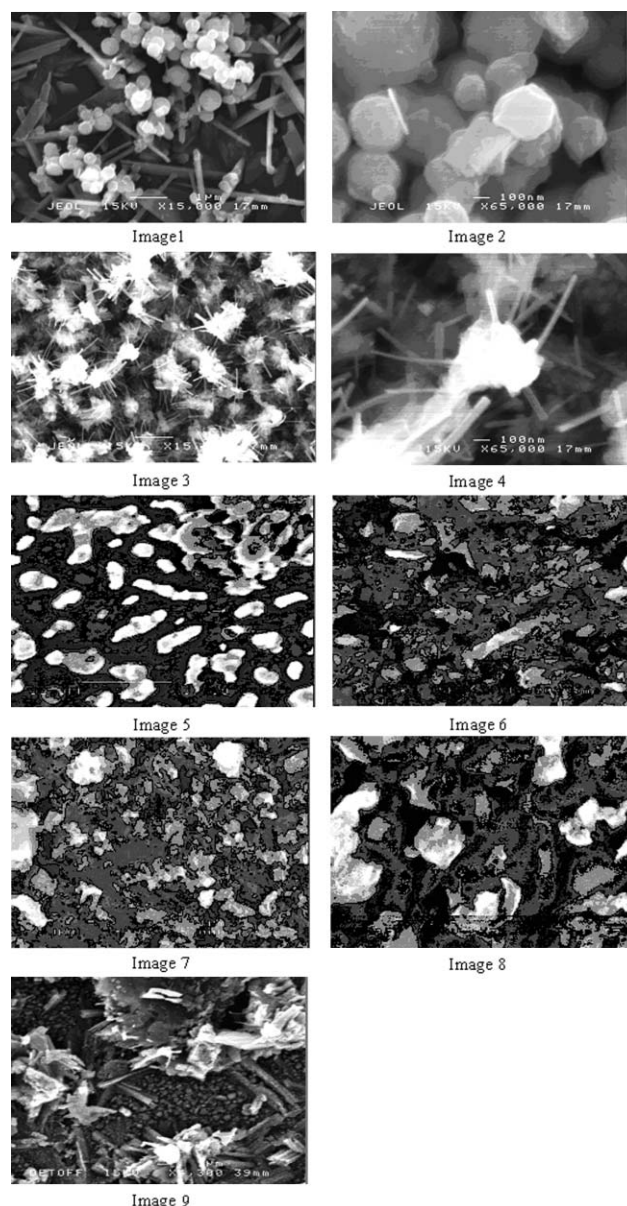


Fig. 6 Scanning electron micrographs of molybdenum oxide films deposited from AACVD reactions of polyoxometallate precursors. Images 1 and 2 show the surface morphology of the coatings deposited from $[\text{Bu}_4\text{N}]_4[\text{Mo}_8\text{O}_{26}]$ at 400 °C, images 3 and 4 at 500 °C and image 5 following annealing in air at 550 °C. Images 6, 7, 8 and 9 show the films deposited from $[\text{Bu}_4\text{N}]_2[\text{Mo}_2\text{O}_7]$, $[\text{Bu}_4\text{N}]_4[\text{Mo}_6\text{O}_{19}]$, $(\text{NH}_4)_6[\text{Mo}_7\text{O}_{24}]$ and $[\text{Bu}_4\text{N}]_3[\text{PMo}_{12}\text{O}_{40}]$ respectively prepared at 550 °C

unlike those seen in literature for films deposited from molybdenum hexacarbonyl and oxygen by APCVD on silicon wafers by molybdenum pentacarbonyl 1-methylbutylisocyanide *via* PECVD on glass and molybdenum pentachloride by means of spray pyrolysis, all of which have a uniform and compact microstructure, similar to that observed upon sintering the polyoxometallate deposited films.^{8,9} The range of different morphologies obtained in this study has important implications for the functional properties of the films, in particular the gas-sensing properties which can be enhanced by an open

porous structure and the hydrophobicity of the films which is dependent upon a needle-like microstructure. Cross-section SEM showed that all the film thicknesses were of the order 500 nm, which correlates to a growth rate of approximately 15 nm min^{-1} .

Wavelength dispersive analysis of the molybdenum oxide films deposited from $[\text{Bu}_4\text{N}]_4[\text{Mo}_8\text{O}_{26}]$, $[\text{Bu}_4\text{N}]_2[\text{Mo}_2\text{O}_7]$, $[\text{Bu}_4\text{N}]_4[\text{Mo}_8\text{O}_{26}]$ and $[\text{NH}_4]_6[\text{Mo}_7\text{O}_{24}]$ showed only the presence of molybdenum and oxygen in the expected ratios (MoO_3 , MoO_2 or a mixed phase). In addition to molybdenum and oxygen significant levels of phosphorus were detected in the WDX spectra for the films obtained from $[\text{Bu}_4\text{N}]_3[\text{PMo}_{12}\text{O}_{40}]$ deposited at $400\text{--}500^\circ\text{C}$ with a Mo : P elemental ratio of 12 : 1, which mirrored the ratio of the starting material. This implies that other polyoxometallates with mixed element cores are likely to serve as suitable precursors for molybdenum oxide films with controlled incorporation of a secondary element.

X-Ray photoelectron analysis. The films obtained from the AACVD reaction of $[\text{Bu}_4\text{N}]_4[\text{Mo}_8\text{O}_{26}]$ in acetonitrile at 400°C and carrier gas flow of 0.5 l min^{-1} were comprised of two distinct regions; a white MoO_3 region closest to the precursor inlet (region A) and a deep blue mixed MoO_3 and MoO_2 phase further away (region B). XPS of region A revealed a doublet corresponding to $\text{Mo}^{6+} 3d_{5/2}$ and $\text{Mo}^{6+} 3d_{3/2}$ photoelectrons at binding energies of 233.1 and 236.3 eV respectively and an O 1s ionisation at 531.0 eV. These molybdenum and oxygen chemical shifts are in good agreement with previous studies of MoO_3 .¹⁶ The absence of any splitting or broadening of the Mo 3d doublet indicates that the Mo was present in a single environment; this is consistent with the Raman and XRD data which showed that the region was comprised solely of the MoO_3 phase. In contrast the Mo 3d doublet for region B was a composite of two peaks: a shoulder is observed at binding energies of 229.4 eV and 232.6 eV, indicative of the presence of MoO_2 , which is again in agreement with the Raman and XRD analysis.

The XPS surface scan of the film deposited from $[\text{Bu}_4\text{N}]_3[\text{PMo}_{12}\text{O}_{40}]$ at 450°C and carrier gas flow of 1 l min^{-1} was similar to that of region B, containing multiple Mo 3d environments at binding energies of 233.0 and 236.1 eV and 232.0 eV and 235.0 eV indicating the presence of a mixed MoO_3 and MoO_2 surface, and O 1s ionisations at 530.9 and 532.0 eV. In addition a P 2p ionisation was observed at 134.2 eV consistent with the presence of MoP_2O_7 , which is in agreement with XRD analysis. The Mo : P ratio was again found to be 12 : 1, the same as in the precursor. Therefore, using $[\text{Bu}_4\text{N}]_3[\text{PMo}_{12}\text{O}_{40}]$ as a precursor has yielded molybdenum oxide composite thin films containing a molybdenum phosphorus oxide, in which the molybdenum to phosphorus ratio of the initial polyoxometallate precursor has been preserved.

Phase variation. Raman and XRD analysis show that low deposition temperatures are favourable for the formation of MoO_3 whereas at high deposition temperatures MoO_2 is the dominant phase. This variation in phase as a function of deposition temperature correlates well with the TGA data

(recorded under a nitrogen atmosphere), which shows that the MoO_3 phase is formed within a narrow temperature range and readily undergoes oxygen loss. However all films are converted to MoO_3 following annealing in air at 600°C , which implies that the oxygen loss is a dynamic process. The variation in phase composition within an individual film is a consequence of the slightly elevated substrate and gas flow temperatures nearer the back of the reactor. This is because the reactor is of a cold wall design and only the substrate plate is heated. The variation in colour from pale yellow to blue with increasing distance from the precursor inlet represents the transition from the MoO_3 phase to MoO_2 . The observation of the pale yellow regions is consistent with the presence of MoO_3 , however MoO_2 is grey. This discrepancy in colour suggests that the blue regions analysed as MoO_2 also contain Mo^{5+} centres such as $\text{MoO}_2(\text{OH})$, which although they are present only in trace amounts as indicated by the lack of any diffraction or spectroscopic evidence have a very intense blue colour and hence dominate over the grey MoO_2 .

Functional properties. The molybdenum oxide films were hydrophobic in nature, with water contact angle values in the range $75\text{--}125^\circ$. The highest contact angles were measured for the films which were comprised of MoO_2 or a mixture of the two oxide phases. SEM showed that these films had a needle-like microstructure, which is indicative of a rough surface (see Fig. 6, image 3). The surfaces were adhesive in that water droplets tended not to be displaced even when placed vertically or inverted. As such they are examples of a Wenzel hydrophobic surface¹⁹ where the water droplet penetrates the surface structure rather than a Cassie–Baxter surface²⁰ where the water droplet is held by the surface and in effect is supported on a cushion of air. We have recently reported water contact angles as high as 145° on a WSe_2 surface, this surface was also very spiky in nature.²¹ Whilst the molybdenum oxide films are not quite as hydrophobic they are easier to produce and do not involve the use of potentially toxic selenium. It is unusual to have contact angles in excess of 110° , in fact commercial lenses for spectacles typically have contact angles of 95° .²¹ The generation of very hydrophobic thin films such as the ones reported here are unsuitable for use in self-cleaning or antimicrobial applications. However they could find application in biology for micropipetting and in microfluidics.

The molybdenum oxide films were also examined as gas sensitive resistors for the detection of ethanol. The molybdenum oxide films were deposited as previously described except that they were laid down on a gas sensor substrate, which consisted of a series of interdigitated gold electrodes on an alumina tile. The molybdenum oxide coating covered both the electrodes and the alumina tile. The thin film responded well to pulses of ethanol (100 ppm level, 50 minutes on and then off) in dry air showing a significant change in resistance (Fig. 7) and recovered to baseline resistance upon removal of the ethanol pulse. The magnitude of the response did not change significantly with each pulse of ethanol with the exception of the initial pulse which was approximately half that of subsequent pulses. We have shown previously that CVD can be used to form gas sensors of tungsten oxide and chromium titanium oxide.²³ The molybdenum oxide sensors formed here

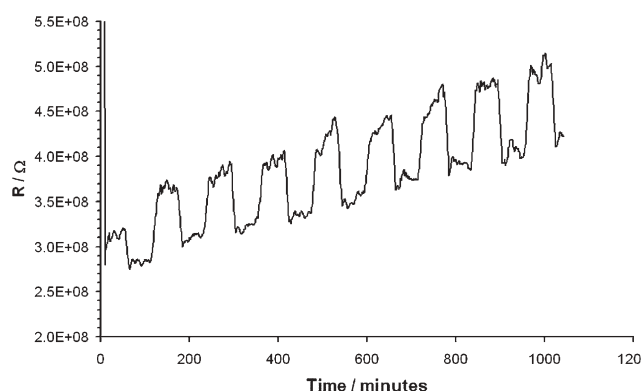


Fig. 7 The change in electrical resistance upon repeated exposure to 100 ppm of ethanol vapour for a gas sensor deposited from $[\text{Bu}_4\text{N}]_3[\text{PMo}_{12}\text{O}_{40}]$ in acetonitrile at 550 °C.

show similar responses to those made previously. One emerging feature of CVD prepared gas sensors is that they tend to have a much denser, less porous microstructure compared with sensors made by screen printing¹³ consequently they tend to have lower overall responses. Advantages that CVD does have over screen printing for making gas sensors include the ease of manufacture and the fact that these films are readily integrable into silicon microfabrication.

Use of an aerosol in CVD

The use of an aerosol in CVD has modified the requirements of the precursor. In traditional molecular organic chemical vapour deposition precursors are designed to be volatile and are often single source such that they contain the bonds required in the growing film in the precursor. For example metal oxide films are typically laid down from metal alkoxides such as $\text{Ti}(\text{O}^i\text{Pr})_4$ and metal nitride films from $\text{Ti}(\text{NMe}_2)_4$.²² In aerosol assisted chemical vapour deposition the primary requirement of the precursor is solubility in a suitable solvent and the ability of the solvent to form a stable aerosol mist. The precursors used in this work are large ionic complexes with very high molecular masses ranging from 788 to 2549 g mol^{-1} that would be unsuitable for use as conventional CVD precursors due to their lack of volatility and thermal stability. However they are readily transported in acetonitrile or water aerosols to the reaction site where the aerosol droplet evaporates depositing the precursor on the surface. It is possible that the formation particularly of the MoO_3 phase occurs partially in the gas phase; this is consistent with the SEM studies which revealed a spherical morphology for this phase. Such a morphology would be expected upon evaporation and condensation of an aerosol droplet, which is in effect a spherical microreactor which decreases in size following evaporation of the solvent. Interestingly the size of these aerosol droplets is *ca.* 15 microns based on the piezoelectric crystal used and the diameter of the MoO_3 particles is in the range between 0.5–1 microns.²³ In this instance however it is some what debatable whether film growth is due to a CVD process. The basis of the growth appears to be evaporation of solvent to produce polyoxometallate clusters which undergo agglomeration, rather than a small molecular unit which is

further vaporised as is the case with conventional AACVD. In conventional aerosol CVD, the solvent is evaporated to leave a small molecular unit that itself is vaporised. Furthermore the effects of thermophoresis are typically negligible. It would appear that formation of nanoparticles in the gas phase and then agglomeration are important which then undergo further reaction (or sintering) as a secondary more CVD like process.

The ease of polyoxometallate formation, the majority of which are standard preparations as reported in *Inorganic Synthesis*,¹² coupled with their clean decomposition to molybdenum oxide makes them desirable for use as novel CVD precursors. The use of the phosphorus doped polyoxometallate, $[\text{Bu}_4\text{N}]_3[\text{PMo}_{12}\text{O}_{40}]$, resulted in the deposition of phosphorus doped molybdenum oxide films in which the Mo : P ratio of the core has been retained. This indicates that it is the polyoxometallate core that determines the secondary element level in the film and could be readily harnessed by using a mixture of polyoxometallate precursors. Furthermore the attendant organic counter ions do not introduce any detectable carbon or nitrogen in the films and correlate well with the TGA plots that show mass losses equivalent to the counter ion removal at *ca.* 250 °C. In addition the main solvent used in these experiments, acetonitrile, must evaporate cleanly as the deposited films are free of carbon contamination. Polyoxometallates are good single source precursors to molybdenum oxide films, since no additional oxygen is available from either the carrier gas stream or the aerosol solvent (in the case of acetonitrile) then the only source of oxygen for the growing films is from the polyoxometallate core.

Conclusion

We have demonstrated the use of large charged clusters as single-source precursors in CVD reactions, where it is the convention to use small, neutral monomers. This has been achieved by taking advantage of the aerosol vaporisation technique, whereby the precursor only has to be soluble in a suitable solvent, and volatility is no longer a requirement, as is the case with conventional CVD processes. AACVD reactions of $[\text{Bu}_4\text{N}]_4[\text{Mo}_8\text{O}_{26}]$, $[(n\text{-C}_4\text{H}_9)_4\text{N}]_4[\text{Mo}_2\text{O}_7]$, $[(n\text{-C}_4\text{H}_9)_4\text{N}]_4[\text{Mo}_6\text{O}_{19}]$, $[\text{NH}_4]_6[\text{Mo}_7\text{O}_{24}]$ and $[\text{Bu}_4\text{N}]_3[\text{PMo}_{12}\text{O}_{40}]$ resulted in the deposition of films comprised of multiple regions corresponding to MoO_3 , MoO_2 and a mixture of these oxides, with the MoO_2 phase predominating with increasing temperature and distance from the reactor inlet. Annealing in air for 30 minutes at 600 °C resulted in the conversion of all films to orthorhombic MoO_3 . The resulting film microstructures were varied, dependent upon both the starting precursor and the deposition temperature and unlike those observed previously in literature reports. The range of film morphologies obtained has important implications for the functional properties, namely the gas sensing and contact angles, upon which film microstructure impacts strongly. The molybdenum oxide films are hydrophobic and function as gas sensitive resistors for detecting traces of ethanol vapour in air.

Previous reports detailing the CVD of molybdenum oxide films have either described dual-source routes or involved the initial deposition of molybdenum metal followed by sintering

in an oxygen atmosphere to yield the oxide.⁹ In contrast polyoxometallates provide a single-source route to the formation of molybdenum oxide films; furthermore they enable controlled levels of a dopant to be incorporated into the film, which may modify its functional properties.

Acknowledgements

The EPSRC is thanked for support. Mr D. Knapp, Mr J. Nolan and Mr D. Morphet are thanked for technical assistance in constructing the CVD rig. Mr R. Palgrave, Dr R. Binions and Mr K. Reeves are thanked for their assistance with XPS, WDX and SEM analysis respectively. Professor K. C. Molloy is thanked for useful discussions. Professor Parkin thanks the Royal Society/Wolfson Trust for a research merit award.

References

- 1 M. J. Davis, G. Benito, D. W. Sheel and M. E. Pemble, *Chem. Vap. Deposition*, 2004, **10**, 29.
- 2 K. D. Lee, *Thin Solid Films*, 1997, **302**, 84.
- 3 K. Hinokuma, K. Kishimoto and T. Kudo, *J. Electrochem. Soc.*, 1994, **141**, 876.
- 4 A. Guerfi and L. A. Dao, *J. Electrochem. Soc.*, 1989, **136**, 2435.
- 5 J. Scarminio, A. Lorcenco and A. Gorenston, *Thin Solid Films*, 1997, **302**, 66.
- 6 M. R. Tubbs, *Phys. Status Solidi A*, 1974, **21**, 253.
- 7 M. S. Burdis and J. R. Siddle, *Thin Solid Films*, 1994, **237**, 320.
- 8 M. A. D. Moraes, B. C. Trasferetti, F. P. Rouxinol and R. Landers, *Chem. Mater.*, 2004, **16**, 513–520.
- 9 T. Ivona, K. A. Gesheva, G. Popkirov, M. Genchevard and T. Tzoetova, *Mater. Sci. Eng., B*, 2005, **119**, 232.
- 10 R. Binions, C. J. Carmalt and I. P. Parkin, *Thin Solid Films*, 2004, **469**, 416.
- 11 W. B. Cross and I. P. Parkin, *Chem. Commun.*, 2003, 1696–1697.
- 12 *Inorganic Synthesis*, ed. A. P. Ginsberg, J. Wiley and Sons, Chichester, 1990, vol. 27, p. 86.
- 13 G. Chabanis, I. P. Parkin and D. E. Williams, *Meas. Sci. Technol.*, 2003, **14**, 76; G. A. Shaw, K. E. Pratt, I. P. Parkin and D. E. Williams, *J. Mater. Chem.*, 2005, **15**, 149; G. A. Shaw, K. E. Pratt, I. P. Parkin and D. E. Williams, *Sens. Actuators, B*, 2005, **104**, 151–162.
- 14 E. Radkov and R. E Beer, *Polyhedron*, 1995, **4**, 2139.
- 15 R. G. Palgrave and I. P. Parkin, *J. Am. Chem. Soc.*, 2006, **128**, 1587.
- 16 K. Gesheva, A. Cziraki, T. Ivanova and A. Szekeres, *Thin Solid Films*, 2005, **492**, 322; J. G. Choi and T. Thompson, *Appl. Surf. Sci.*, 1996, **93**, 143.
- 17 N. Wooster, *Z. Kristallogr. Kristallgeom. Kristallphys. Kristallchem.*, 1931, **80**, 504–512.
- 18 A. Magneli, *Ark. Kemi, Mineral. Geol.*, 1947, **24**, 1–11.
- 19 R. N. Wenzel, *Ind. Eng. Chem.*, 1936, **28**, 988.
- 20 A. B. D. Cassie and S. Baxter, *Trans. Faraday Soc.*, 1944, **40**, 546.
- 21 I. P. Parkin and R. G. Palgrave, *J. Mater. Chem.*, 2005, **15**, 1689.
- 22 J. R. Roos and H. Veltrop, *Thin Solid Films*, 1990, **193**, 547.
- 23 G. A. Shaw, K. E. Pratt, I. P. Parkin and D. E. Williams, *Sens. Actuators, B*, 2005, **104**, 151; G. A. Shaw, K. E. Pratt, I. P. Parkin and D. E. Williams, *J. Mater. Chem.*, 2005, **15**, 149.